Turkish Journal of Remote Sensing 8 (2026) 1800982 Research Article

TURKISH JOURNAL OF REMOTE SENSING (Türkiye Uzaktan Algılama Dergisi)
e-ISSN 2687-4997 https://dergipark.org.tr/en/pub/tuzal

Detection of reclamation-induced ground deformation with GACOS-corrected StaMPS PSI: Case study Hatay Airport

Mahmut Görken[*1], **Umut Güneş Sefercik**[2], **Mertcan Nazar**[2]

[1] *Yozgat Bozok University, Şefaatli Vocational School Architecture and Urban Planning, Land Registry and Cadastre Program, Yozgat, Türkiye;* mahmut.gorken@bozok.edu.tr
[2] *Gebze Technical University, Department of Geomatics Engineering, Kocaeli, Türkiye;* sefercik@gtu.edu.tr; mnazar@gtu.edu.tr

Check for updates

Article History:
Received: 10 October 2025
Revised: 21 November 2025
Accepted: 5 December 2025
Published: 25 March 2026

Abstract: Many coastal cities around the globe have initiated construction projects in reclaimed areas with the objective of constructing airports and expanding air transportation services. The looseness of soil structures in reclaimed lands can result in deformations in infrastructure and structures above. It is therefore crucial to implement effective detection and monitoring procedures to identify and assess such deformations. In this study, 151 Sentinel-1A single-look complex (SLC) images, obtained between 2 December 2017 and 29 January 2023, were employed for the purpose of detecting reclamation-induced ground deformation at Hatay Airport using persistent scatterer interferometry (PSI), a multi-temporal interferometric synthetic aperture radar (MT-InSAR) method, through the Stanford Method for Persistent Scatterers (StaMPS) software. Furthermore, the atmospheric phase delay contributions were corrected through the implementation of the Generic Atmospheric Correction Online Service for InSAR (GACOS) data using the Toolbox for Reducing Atmospheric InSAR Noise (TRAIN). The average line-of-sight (LOS) deformation velocity across the area was determined to be between -6.25 mm/year and 9.02 mm/year, with fluctuations observed. The deformation trend observed on the northern and southern sides exhibited disparate directionalities with respect to the LOS. Areas exhibiting a deficiency in PS points relative to the remainder of the dataset may be attributed to the presence of low coherence signals. The application of StaMPS PSI for the monitoring of ground deformation demonstrated an overall accuracy of sub-centimeter measurements in a reclaimed airport area. Overall, the application of MT-InSAR techniques, particularly StaMPS PSI combined with GACOS corrections, enabled the robust detection and monitoring of ground deformation patterns with remarkable precision. This advanced approach is essential for maintenance planning, safety management, and risk mitigation in critical infrastructures such as airports. Early identification of deformation allows for timely intervention, helping to safeguard both structural integrity and operational continuity, thus contributing to the long-term safety and resilience of these strategically important facilities.

Keywords: InSAR; StaMPS PSI; GACOS; deformation monitoring; reclaimed airport

Citation: Görken, M., Sefercik, U. G., & Nazar, M. (2026). Detection of reclamation-induced ground deformation with GACOS-corrected StaMPS PSI: Case study Hatay Airport. *Turk. J. Remote Sens.*, 8, 1800982. https://doi.org/10.51489/tuzal.1800982

1. Introduction

Many coastal communities globally continue to engage in land reclamation efforts due to insufficient room for their expanding populations. In many cases, these projects require extensive modification of existing terrain, and the areas selected for reclamation often include former agricultural fields, shallow coastal flats, and occasionally the beds of rivers or lakes (Martín Antón et al., 2016). Although such interventions provide additional land for urban expansion and infrastructure development, they also introduce a set of geotechnical difficulties that are not always straightforward to manage. Reclaimed ground may experience uneven consolidation due to differences in material composition, groundwater conditions, or the methods used during filling. This can cause subsidence, cracking, or other types of instability over time (Shi et al., 2023). The importance of these challenges becomes particularly evident in regions where critical infrastructure relies on the reliability of the ground conditions. Airports constructed on reclaimed land exhibit an increased sensitivity to these conditions, as the stability of their pavements, runways, and structural facilities relies on consistent and dependable ground behavior to ensure smooth and uninterrupted operations. Consequently, establishing a reliable and ongoing system for monitoring deformation is of utmost importance. Identifying even minor changes at an early stage is crucial for ensuring operational safety. This proactive strategy helps to reduce potential risks and improve the long-term resilience and reliability of airport infrastructure (Bao et al., 2022).

Despite the high precision provided by traditional ground deformation monitoring techniques, their implementation necessitates a considerable investment of labor, can require an extended period of time, and is constrained by low coverage capability for the identification of surface deformation at large scales (Buzzanga et al., 2020). Synthetic aperture radar (SAR) technology has been in extensive use for several decades as an effective tool for generating three-dimensional (3D) models of the Earth and monitoring surface deformation with a high degree of precision, down to a few centimeters. Based on interpreting phase differences between consecutive SAR images, interferometric synthetic aperture radar (InSAR) has become an invaluable method in this regard (Lu et al., 2007; Sefercik, 2013; Biggs & Wright, 2020; Sefercik et al., 2020). Additionally, the differential InSAR (DInSAR) technique employs InSAR technology to derive ground displacement within the radar line-of-sight (LOS) direction by analyzing phase differences between SAR data acquired at different times and from varying orbiting platforms (Pepe et al., 2016). DInSAR method is extensively employed in studies concerning analysis of ground displacements resulting from natural disasters such as earthquakes (Doğanalp et al., 2024; Karca & Erten, 2023). To address the inherent constraints of the DInSAR methodology, including decorrelation, sensitivity to atmospheric fluctuations, and alterations in orbital paths, the multi-temporal InSAR (MT-InSAR) methodology was proposed as a solution for monitoring ground deformation across diverse timeframes (Massonnet & Feigl, 1998; Hooper, 2008; Cigna et al., 2011).

A MT-InSAR method, known as persistent scatterer interferometry (PSI), was devised for monitoring ground displacements with sub-centimeter accuracy through the use of highly coherent persistent scatterer (PS) targets (Ferretti et al., 2001; Ferretti et al., 2000). The Stanford Method for Persistent Scatterers (StaMPS) technique was developed as a means of enhancing the detection capability of PSI for low-amplitude observation points (Hooper et al., 2004). In addition to solely utilizing PS points, there are approaches that integrate both PS and distributed scatterer (DS) points to maximize the ground deformation detecting capabilities of StaMPS (Zhao et al., 2019). The small baseline subset (SBAS) method is another MT-InSAR technique that utilizes SAR images with minimal baselines, employing singular value decomposition (SVD) to enhance spatial correlation and temporal sampling rate (Berardino et al., 2002). Initially developed for detecting large-scale deformations, SBAS has been enhanced by including both multilook and single-look datasets to evaluate the temporal progression of deformation patterns at localized sizes (Lanari et al., 2004). Moreover, a number of methodologies have been proposed to address the issue of atmospheric phase delay error. One such methodology is the recently introduced Generic Atmospheric Correction Online Service for InSAR (GACOS), which employs a tropospheric decomposition (ITD) model based on iterations (Yu et al., 2017a; Yu et al., 2017b; Yu et al., 2018).

In this study, the reclamation-induced ground deformation at Hatay Airport was detected by the utilization of StaMPS PSI with 151 Sentinel 1A single look complex (SLC) images, obtained between 2 December 2017 and 29 January 2023. This dataset offers a sufficiently detailed temporal record that allows for the examination of long-term deformation patterns related to reclaimed ground. The extensive array of acquisitions enables consistent tracking of variations in surface motion. Furthermore, the impact of atmospheric phase delay was assessed, and appropriate corrections were made using GACOS to guarantee that the final phase estimates accurately represented actual ground motion.

2. Study Area and Dataset

The Hatay Airport is located in the northeastern region of Antakya, Hatay Province, Türkiye, at 36°21'46.0"N and 36°16'56.0"E. Moreover, the airport is located 25 km from the city center and comprises a total terminal area of 46826 m^2. The airport is equipped with a single concrete runway, designated as 04/22, which measures 3000 m x 45 m. The airport was built over an area measuring approximately 2.70 km^2 on the site of the now-drained Lake Amik basin. The current land cover of the region surrounding the airport comprises agricultural areas, urban zones, and roadways, with the majority consisting of crop fields and rural settlements. The official inauguration of Hatay Airport was in 2007. The Hatay Airport area is illustrated in Figure 1.

The Sentinel-1 mission was initiated on 3 April 2014 while being operated by the European Space Agency (ESA) within the context of the Copernicus Programme (ESA, 2025). The first Sentinel-1 mission included two sun-synchronous polar-orbiting satellites: Sentinel-1A, which was launched on April 3, 2014, and Sentinel-1B, which was launched on April 25, 2016. However, the Sentinel-1B spacecraft encountered a power supply failure, leading to the cessation of operational functionality on 23 December 2021, and the mission was officially terminated on 3 August 2022, extending the repetition cycle from six days to twelve days. As of 5 December 2024, Sentinel-1C was launched, which increased the temporal resolution to six days. A complete Sentinel-1A SLC dataset was put together for the Hatay Airport area in order to meet the goals of this investigation. The SAR images, acquired in descending orbit with the interferometric wide swath (IW) mode between 2 December 2017 and 29 January 2023, were collected exclusively in vertical-vertical (VV) polarization to optimize sensitivity to ground deformation. The data utilized in this study were obtained from the Alaska Satellite Facility's (ASF) Vertex platform, which guarantees high-quality and consistent imagery. In addition, Shuttle Radar Topography Mission (SRTM) 3 arc-sec (~90 m) digital elevation model (DEM) and GACOS data were utilized in StaMPS PSI processing. Table 1 summarizes the main features of the dataset, which gives a strong base for PSI-based analysis and a correct understanding of how the ground is changing at this complicated infrastructure site.

Figure 1. The Hatay Airport is situated within the Hatay Province, which is located in the southern region of Türkiye

Table 1. The properties of the utilized Sentinel-1A SLC dataset of 151 SAR images obtained between 2 December 2017 and 29 January 2023

Property	Description
Product type	Sentinel-1A TOPS SLC
Wavelength	C-band/5.55 cm
Acquisition date	20171202-20230129
Number of images	151
Acquisition mode	IW
Orbit direction	Descending
Polarization	VV
Path/Frame No.	21/14
Spatial resolution	5 m (ground range) x 20 m (azimuth)
Pixel spacing	2.3 m (slant range) x 14.1 m (azimuth)
Incidence angle	29°-46°
Total swath width	250 km

3. Methodology

The methodology of this study comprises two stages: the initial pre-processing of the Sentinel-1A dataset and the subsequent StaMPS PSI processing, which are illustrated in Figure 2. The latter entailed the implementation of atmospheric phase delay correction utilizing GACOS products. The pre-processing of the StaMPS PSI was executed with the use of SNAP 9.0.0, a toolbox designed for the Sentinel-1A data, developed by the ESA.

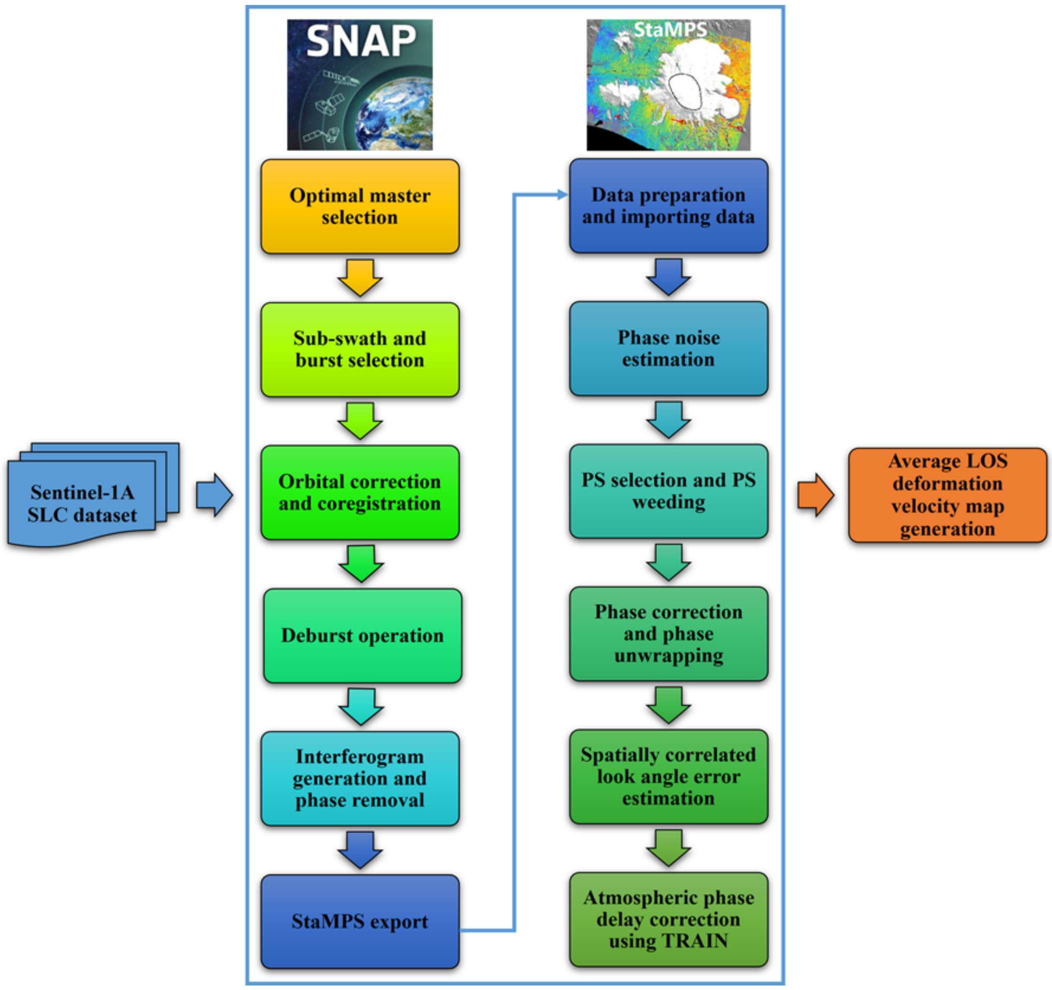

Figure 2. The study methodology comprises two stages: the initial pre-processing of the Sentinel-1A dataset and the subsequent StaMPS PSI processing

The optimal master selection represents a pivotal stage in the interferogram generation process, as all subsequent processing of slave images is contingent upon the selected master.

In addition, the selection of the master image has a direct impact on the quality of the interferograms, which in turn affects the accuracy of the deformation analysis. When selecting the master image, a number of parameters are taken into account. The aforementioned parameters are the perpendicular baseline, the temporal baseline, the Doppler centroid frequency difference, and the height ambiguity. The perpendicular base length is the spatial distance between two SAR images and is of great importance in InSAR analyses. This spatial distance is the perpendicular distance between the positions of the radar antennas at the time of acquisition of two SAR images obtained at different times. In other words, it is the distance perpendicular to the orbital plane. If this distance is large, geometric differences between the two images may occur, which has a negative effect on the quality of the interferograms by reducing the coherence between the images. The temporal baseline is the interval between the acquisition dates of two SAR images and is typically expressed in days. A high or low temporal baseline can impact the quality of the interferogram. A high temporal baseline allows for the detailed observation of deformation, whereas a low temporal baseline may result in insufficient deformation detection. It is therefore important to ensure that the temporal baseline of the master image with other images is optimal.

The mean Doppler centroid frequency difference is defined as the difference between the mean Doppler centroid frequencies observed in two distinct SAR images. These frequencies represent the shifts in frequency that occur between the time the signal is reflected from the target objects and the time it is recorded. The primary cause of these frequency shifts is the movement of the radar antenna and the target objects. The selection of the image with a low Doppler centroid frequency difference as the master has a beneficial impact on the quality of the interferograms and enhances the reliability of the analyses. Height ambiguity is defined as the change in height corresponding to the phase altitude. It is inversely proportional to the vertical base length. In order to generate interferograms with high sensitivity to height variations, it is necessary to select an image with low height ambiguity as the master image. In accordance with the parameters employed, the image exhibiting the highest correlation with the image stack is designated as the master image (Hooper et al., 2004; Ferretti et al., 2004; Kampes & Hanssen, 2004; Chen et al., 2007; Liu et al., 2018). This operation was carried out in strict adherence to the stipulation of achieving a requisite level of geometric and temporal decorrelation (Ferretti et al., 2000; Rucci et al., 2012). In light of the previously outlined prerequisites, the master image was identified as the one acquired on 29 September 2020. The remaining processes were executed in the SNAP Graph Builder operator, thus enabling users to construct sequences of processing commands or graphs that can be applied in bulk through the Graph Processing Tool (GPT).

Once the optimal master image was selected, the subsequent steps involved the initiation of the sub-swath and burst selection and the orbital correction processes. In these phases, the Terrain Observation with Progressive Scans SAR (TOPSAR) Split and Apply Orbit operations were executed initially. The TOPSAR Split operation was employed for the purpose of dividing the bursts within the workspace. This results in a reduction in data volume and a concomitant reduction in processing time. Subsequently, the Apply Orbit operation was performed. This process is fundamental to ensuring the accurate geocoding of the images. In the course of the aforementioned process, the orbit data, which comprises the position of the satellite at the time of acquisition, is applied to the images. This was achieved through the utilization of precise orbit files provided by the ESA. The precise orbit files contain detailed information regarding the precise trajectory of the satellite, which enables more accurate alignment of the images. Subsequently, the process of back geocoding was undertaken for the purpose of coregistration. This process entails the conversion of all images from the radar coordinate system to the geographic coordinate system. Accordingly, the georeferenced images were aligned with one another in accordance with the master image and then stacked into a single stack. In the event that the study area is situated within multiple bursts or if there is a necessity to consolidate successive bursts into a single image, the deburst process is employed. During this process, all bursts are resampled in both the distance and azimuth directions. In the direction, all bursts and aligned side bursts are merged at a common time (t), with the merging process performed from the center of the bursts for overlapping areas. In the azimuth direction, the bursts are merged according to zero Doppler time. The aforementioned process was conducted utilizing the TOPS deburst operator within the SNAP toolbox.

Once the images were accurately matched, aligned, and debursted, the interferogram generation step was initiated. An interferogram is defined as an image formed by comparing the phase information of at least two SAR images. The use of interferograms containing phase differences in SAR images is a valuable tool for the detection of surface deformations. In the generation of interferograms, a total of n SAR images were employed, resulting in the production of n-1 interferograms with the master image selected as the reference. In the present study, a total of 150 interferograms were generated from 151 SAR images. Furthermore, the interferogram generation process entailed the removal of both the flat-earth phase and the topographic phase. The flat-earth phase is a consequence of the curvature of the observed surface and can be estimated utilizing orbital and metadata information. In the removal of the topographic phase step, the topographic phase component, which is an additive component in the phase difference mentioned in the interferogram generation step, was removed. The aforementioned additive component is typically removed through the utilization of a reference DEM. This process was conducted using the DEM generated by the SRTM, which is accessible in numerous software applications. The SRTM dataset encompasses a latitudinal range between 60° north and 56° south, encompassing approximately 80% of the Earth's surface. The sampling interval is 3 arc-sec, which equates to approximately 90 m x 90 m. Additionally, a resolution of 1 arc-sec is available. Finally, as the last step in the pre-processing of the Sentinel-1A dataset, the StaMPS export was performed.

The PSI processing was carried out using the StaMPS 4.1b software, which is available at the GitHub repository (https://github.com/dbekaert/StaMPS). The processing steps of the StaMPS PSI methodology were applied through the MATLAB R2022b environment on an Ubuntu 18.04.6 LTS virtual machine. The selection procedure for the PS candidate was carried out by utilizing a default threshold of 0.4 for pixel amplitude dispersion value (Hooper, 2008). The selection of PS candidates in existing methods is contingent upon the implementation of a threshold for pixel amplitude dispersion values (Ferretti et al., 2001).

$$D_A = \frac{\sigma_A}{\mu_A} \tag{1}$$

Where D_A represents the amplitude dispersion index, while σ_A represents the standard deviation of the amplitude values, and μ_A represents the mean of the amplitude values. Subsequent to the preliminary selection of PS candidates, the StaMPS processing steps from 1 to 7, as delineated in the StaMPS/MTI manual (Version 4.1b) (Hooper et al., 2004), were undertaken. As an alternative approach to step 8, the atmospheric phase delay was corrected using the Toolbox for Reducing Atmospheric InSAR Noise (TRAIN) (Bekaert et al., 2015a; Bekaert et al., 2015b). The TRAIN toolbox module is compatible with StaMPS and has been developed at the University of Leeds. The GACOS products were imported into TRAIN (Version 3beta), which is available at the GitHub repository (https://github.com/dbekaert/TRAIN). In the StaMPS PSI processing, the initial step involved the preparation and importation of data, which was carried out by applying the script mt_prep_snap with the default StaMPS PSI processing parameters. These included D_A as 0.4, the number of patches in the range as 1, the number of patches in azimuth as 1, the overlapping pixels between patches in the range as 50, and the overlapping pixels between patches in azimuth as 200. Subsequently, phase noise estimation was conducted. Phase noise estimation is a process that improves the reliability of interferograms by making the phase information more precise. It is an important step for better detection of surface deformations. Phase noise can be caused by various factors, including atmospheric effects, sensor errors, and geometrical errors. The software evaluates phase and amplitude information and performs noise estimation using various filters. Additionally, in this step, the estimation of PS candidates is also performed. PS points demonstrate high phase stability. Phase stability can be ascertained by removing the components, which include errors caused by the atmospheric phase screen (APS) and DEM.

Targets with high geometric and temporal correlation are considered PS candidates, and pixels with constant amplitude values are deemed to have PS potential. Following the necessary operations among the PS candidates formed by phase estimation, PS selection is performed. Points with values that fall below the predetermined D_A value are designated as PS. The D_A value establishes a threshold such that pixels exhibiting irregular amplitude, including those representing the water surface and vegetation, are excluded from the PS selection process. According to the StaMPS manual, the D_A value is recommended to be set within the range of 0.4–0.42, while (Hooper et al., 2007) suggested that values up to 0.6 may still correspond to signals distinguishable from noise. As this value increases, the number of processed pixels will also increase. During PS selection, PS points that exceed the correlation and amplitude dispersion threshold are eliminated. Furthermore, the phase changes of the PS points in the time series are evaluated, and PS points with low phase stability are also excluded. Finally, those with high phase standard deviation among the PS points are removed, and the extraction is completed.

Phase unwrapping was conducted using the 3D phase unwrapping technique. In the 3D phase unwrapping technique, two dimensions are used to represent the spatial component, while the remaining dimension represents the temporal component. Firstly, phase unwrapping is performed in the time dimension of all PS pixels representing PS points. This process is conducted using time series or phase modeling techniques. Subsequently, the phase differences resolved in the time dimension are spatially phase unwrapped using an iterative algorithm for each time step. This process is performed using phase differences between neighboring pixels. Finally, the process is completed by integrating the location and time dimensions. The unwrapped phase encompasses a number of components, including spatially correlated looking angle (SCLA) error, atmospheric error, and orbital error. SCLA pertains to the spatial correlation of the viewpoint from which SAR images are acquired. This error is attributable to a number of factors, including the geometry of the SAR image, topographic elevation changes, and atmospheric conditions. It can be rectified through the utilization of topographic and atmospheric models.

In the phase delay correction stage, the contributions of atmospheric and orbital errors were first estimated and then removed to ensure that the remaining phase signal accurately represented ground deformation. This correction relied on atmospheric filtering techniques, which are commonly used to identify and reduce phase distortions introduced by variations in atmospheric conditions. Atmospheric filtering aims to separate these unwanted components from the deformation signal by modelling the behaviour of atmospheric delays, which mainly consist of tropospheric and ionospheric effects. Among these, the tropospheric delay is generally the more influential component in InSAR processing and therefore requires particular attention during correction. To address these issues, a combination of spatial, temporal, and height-based filtering strategies was applied to isolate and suppress the atmospheric contributions. The TRAIN module is frequently used for estimating and removing tropospheric delays, as it is capable of incorporating external atmospheric models in the correction workflow. In this study, GACOS data were integrated into TRAIN to support the estimation of tropospheric delay and to refine the phase observations accordingly. Once the filtering process was completed, the corrected phase information enabled the creation of an average LOS deformation velocity map, which then formed the basis for the following stages of interpretation and analysis. This map provided a clearer view of the spatial pattern of LOS motion across the airport area and guided the identification of zones showing notable displacement behavior.

4. Results and Discussion

A total of 4041 PS points were identified through the processing of the Sentinel 1A SLC dataset by StaMPS PSI, as illustrated in Figure 3. This distribution reflects the availability of coherent scatterers across the broader study region and indicates that a sufficient number of stable radar targets were preserved throughout the observation period. Within the boundaries of Hatay Airport itself, 1627 PS points were detected. This subset forms the core of the deformation analysis, since these points directly represent LOS motion on the airport platform and provide the spatial density needed to examine local variations in ground behavior across the reclaimed area.

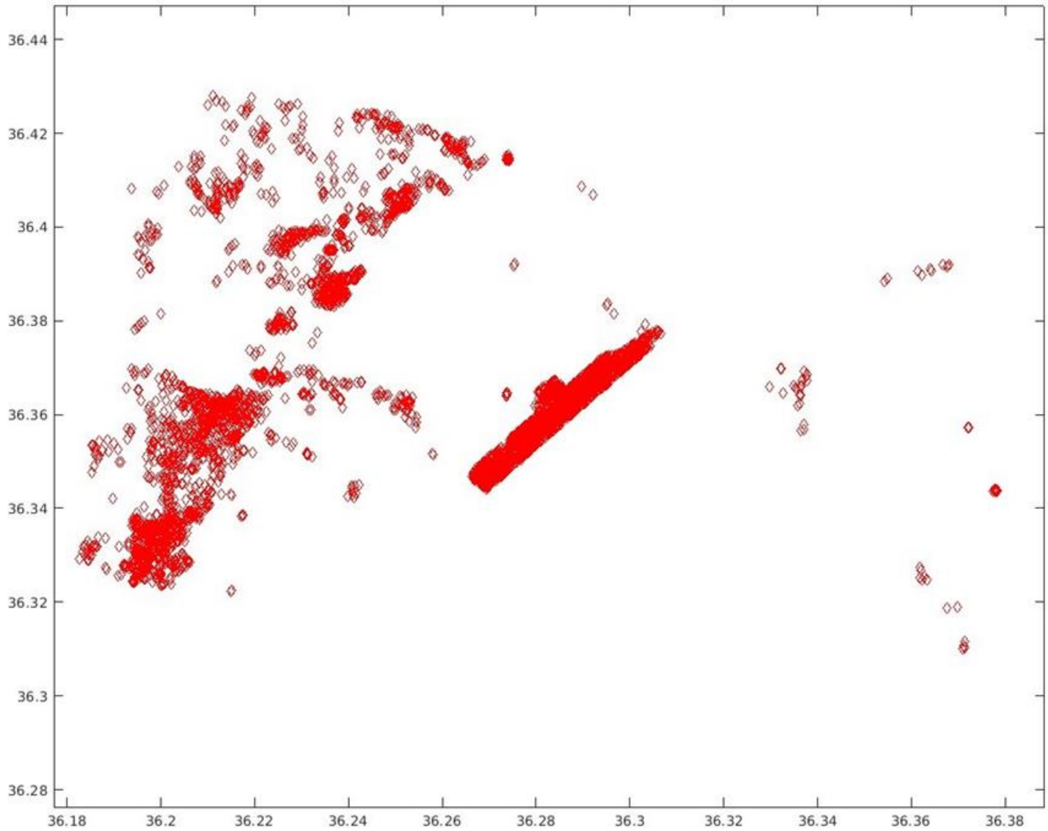

Figure 3. Distribution of the 4041 PS points detected by StaMPS PSI processing of the Sentinel-1A SLC dataset, the coordinate system is the World Geodetic System 1984 (WGS84)

The resulting average LOS deformation velocity map for Hatay Airport is presented in Figure 4. The spatial pattern displayed in the figure shows considerable variation across the airport platform, with LOS deformation velocities ranging from roughly -6.25 mm/year to 9.02 mm/year. These variations indicate that different parts of the airport are moving at different rates along the radar LOS. Some areas exhibit motion directed toward the satellite, whereas others show movement away from the satellite. This behavior reflects changes in the LOS component of ground displacement rather than true vertical uplift or settlement, underscoring the need for careful interpretation of deformation signals in complex reclaimed ground environments.

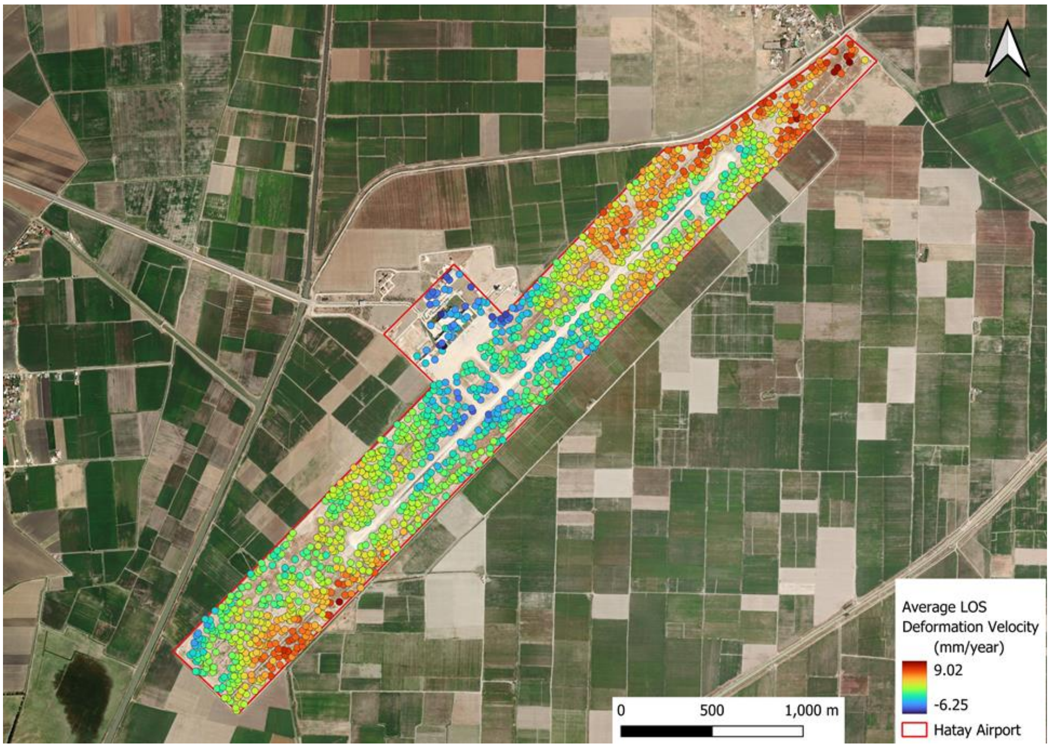

Figure 4. The average LOS deformation velocity map of Hatay Airport was generated using the GACOS-corrected StaMPS PSI processing of the Sentinel-1A SLC dataset

The average LOS velocities in the northern portion of the airport show movement in the direction of the satellite, indicating either ground rebound or uplift. On the other hand, the southern sector moved away from the satellite, a phenomenon typically associated with settlement or subsidence. The distinct geotechnical or hydrological processes at work, which may be influenced by the underlying conditions or human activity in the airport area, may be indicated by the variations in deformation trajectories from north to south.

An intriguing result of the analysis is that, in comparison to other areas within the airport boundary, the flat runway and terminal zones have a significantly lower density of PS points. This reduction in point density can be linked to the presence of planted lawns and moist, unconsolidated soils commonly found in these areas. Such land cover is known to reduce the temporal coherence necessary for StaMPS PSI, limiting the identification of reliable scatterers. In particular, reclaimed or artificially constructed zones within the airport, which often contain freshly planted grass or poorly compacted soils, are especially susceptible to coherence loss (Jiang et al., 2016). As a result, these sections tend to yield fewer PS points, reducing the spatial detail and reliability of the deformation measurements.

This finding underscores a known limitation of StaMPS PSI when applied to environments dominated by vegetation or variable soil moisture. In such cases, the point density and quality of deformation estimates may be significantly constrained, emphasizing the importance of integrating additional data sources or alternative remote sensing methods when monitoring ground motion in complex, dynamic landscapes such as airport environments. Additionally, the utilization of alternative MT-InSAR methods can be considered for further analysis, especially to validate the robustness of the deformation signals and to provide complementary insights into spatial or temporal patterns.

5. Conclusions

Due to the difficult subsurface conditions typical of such environments, the risk of deformation developing over time in major engineering structures like motorways, bridges, and airports built on reclaimed wetlands continues to be a major concern. Advanced observation technologies are regularly used in many developed nations to monitor the stability and health of these massive structures, guaranteeing the early detection of any potentially dangerous ground movements. In this regard, Hatay Airport is a crucial location for deformation monitoring studies since it is one of the largest engineering projects built on reclaimed land in Turkey.

This study explores the ground deformation occurring at Hatay Airport by utilizing GACOS-corrected StaMPS PSI processing on Sentinel-1A data. The analysis employed a thorough dataset, consisting of 151 images gathered from 2 December 2017 to 29 January 2023. This method allowed for a detailed mapping of the spatial variations in average deformation velocity of the land surface across the airport. The results demonstrated distinct differences in the average LOS deformation velocities between the northern and southern parts of the airport. The northern section indicated a shift toward the satellite, implying a process of uplift or ground recovery. In contrast, the southern part exhibited movement away from the satellite, which corresponds with subsidence or settlement phenomena. The observed average deformation velocities for land subsidence ranged from -6.25 mm/year to 9.02 mm/year, underscoring the complex and dynamic nature of ground movement in reclaimed airport environments.

This study highlights the significant use of MT-InSAR methods, which enable tracking of ground movement with remarkable sub-centimeter accuracy. The remarkable precision achieved in this context holds significant importance for airport management. It allows for the prompt detection of potentially concerning deformations, thereby preventing any operational or structural risks that may arise. The integration of StaMPS PSI and GACOS atmospheric correction demonstrates significant effectiveness in minimizing noise and improving the reliability of deformation measurements. This is particularly noteworthy in regions where low coherence, caused by factors such as vegetation or soil moisture, could otherwise restrict the availability of usable PS points. In these parts of the scene, coherence often fluctuates between acquisitions, and the number of stable scatterers drops quickly.

The findings highlight the critical need for ongoing and attentive monitoring in large infrastructure projects constructed on reclaimed lands. The use of MT-InSAR techniques, like StaMPS PSI, especially when enhanced with GACOS corrections, allows for a reliable identification and evaluation of ground deformation patterns. This offers essential assistance for planning maintenance, managing safety, and preventing risks in important facilities such as airports. Ultimately, it enhances the long-term resilience and operational safety of these crucial transportation centers.

Acknowledgments: The authors acknowledged that this study is derived from the PhD Thesis of Mahmut Gorken.

No artificial intelligence tools were used in the preparation of this manuscript.

Author Contributions:
M. Gorken: Data curation, Conceptualization, Investigation, Methodology, Writing—original draft preparation, Writing—reviewing and editing, Software.
U. G. Sefercik: Data curation, Conceptualization, Investigation, Methodology, Writing—original draft preparation, Writing—reviewing and editing, Software, Validation.
M. Nazar: Data curation, Conceptualization, Investigation, Methodology, Writing—original draft preparation, Writing—reviewing and editing, Software.

Funding: The author declares that there is no financial support.

Research and publication ethics statement: In the study, the authors declare that there is no violation of research and publication ethics and that the study does not require ethics committee approval.

Conflicts of Interest: The authors declare no conflicts of interest.

Data Availability: The data presented in this study are available on request from the corresponding author.

References

Bao, X., Zhang, R., Shama, A., Li, S., Xie, L., Lv, J., Fu, Y., Wu, R., & Liu, G. (2022). Ground deformation pattern analysis and evolution prediction of Shanghai Pudong International Airport based on PSI long time series observations. *Remote Sensing*, 14(3), 610. https://doi.org/10.3390/rs14030610

Bekaert, D. P. S., Hooper, A., & Wright, T. J. (2015a). A spatially variable power law tropospheric correction technique for InSAR data. *Journal of Geophysical Research: Solid Earth*, 120(2), 1345–1356. https://doi.org/10.1002/2014jb011558

Bekaert, D. P. S., Walters, R. J., Wright, T. J., Hooper, A. J., & Parker, D. J. (2015b). Statistical comparison of InSAR tropospheric correction techniques. *Remote Sensing of Environment*, 170, 40–47. https://doi.org/10.1016/j.rse.2015.08.035

Berardino, P., Fornaro, G., Lanari, R., & Sansosti, E. (2002). A new algorithm for surface deformation monitoring based on small baseline differential SAR interferograms. *IEEE Transactions on Geoscience and Remote Sensing*, 40(11), 2375-2383. https://doi.org/10.1109/TGRS.2002.803792

Biggs, J., & Wright, T. J. (2020). How satellite InSAR has grown from opportunistic science to routine monitoring over the last decade. *Nature Communications*, 11(1), 3863. https://doi.org/10.1038/s41467-020-17587-6

Buzzanga, B., Bekaert, D. P. S., Hamlington, B. D., & Sangha, S. S. (2020). Toward sustained monitoring of subsidence at the coast using InSAR and GPS: An application in Hampton Roads, Virginia. *Geophysical Research Letters*, 47(18), e2020GL090013. https://doi.org/10.1029/2020gl090013

Chen, Q., Ding, X., & Liu, G. X. (2007). Method for optimum selection of common master acquisition for PS-DInSAR. *Acta Geodaetica et Cartographica Sinica*, 36(4), 395–399.

Cigna, F., Del Ventisette, C., Liguori, V., & Casagli, N. (2011). Advanced radar-interpretation of InSAR time series for mapping and characterization of geological processes. *Natural Hazards and Earth System Sciences*, 11(3), 865–881. https://doi.org/10.5194/nhess-11-865-2011

Doğanalp, S., Coşkuner, B., & Makineci, H. B. (2024). Analysis of short-term Sentinel-1 data using the DInSAR method for monitoring displacement following the earthquakes of 6 and 20 February in Hatay city. *Bulletin of Geophysics & Oceanography*, 65(4), 491-512. https://doi.org/10.4430/bgo00478

ESA. (2025). Retrieved October 10, 2025, from https://sentiwiki.copernicus.eu/web/s1-mission

Ferretti, A., Novali, F., Bürgmann, R., Hilley, G., & Prati, C. (2004). InSAR permanent scatterer analysis reveals ups and downs in San Francisco Bay Area. *Eos, Transactions American Geophysical Union*, 85(34), 317–324. https://doi.org/10.1029/2004eo340002

Ferretti, A., Prati, C., & Rocca, F. (2000). Nonlinear subsidence rate estimation using permanent scatterers in differential SAR interferometry. *IEEE Transactions on Geoscience and Remote Sensing*, 38(5), 2202–2212. https://doi.org/10.1109/36.868878

Ferretti, A., Prati, C., & Rocca, F. (2001). Permanent scatterers in SAR interferometry. *IEEE Transactions on Geoscience and Remote Sensing*, 39(1), 8–20. https://doi.org/10.1109/36.898661

Hooper, A. (2008). A multi-temporal InSAR method incorporating both persistent scatterer and small baseline approaches. *Geophysical Research Letters*, 35(16). https://doi.org/10.1029/2008gl034654

Hooper, A., Bekaert, D., Hussain, E., & Spaans, K. (2018). StaMPS/MTI Manual (Version 4.1b). University of Leeds, UK. Retrieved October 10, 2025, from https://homepages.see.leeds.ac.uk/~earahoo/stamps/StaMPS_Manual_v4.1b1.pdf

Hooper, A., Segall, P., & Zebker, H. (2007). Persistent scatterer interferometric synthetic aperture radar for crustal deformation analysis, with application to Volcán Alcedo, Galápagos. *Journal of Geophysical Research: Solid Earth*, 112(B7). https://doi.org/10.1029/2006JB004763

Hooper, A., Zebker, H., Segall, P., & Kampes, B. (2004). A new method for measuring deformation on volcanoes and other natural terrains using InSAR persistent scatterers. *Geophysical Research Letters*, 31(23). https://doi.org/10.1029/2004gl021737

Jiang, Y., Liao, M., Wang, H., Zhang, L., & Balz, T. (2016). Deformation monitoring and analysis of the geological environment of Pudong International Airport with persistent scatterer SAR interferometry. *Remote Sensing*, 8(12), 1021. https://doi.org/10.3390/rs8121021

Kampes, B. M., & Hanssen, R. F. (2004). Ambiguity resolution for permanent scatterer interferometry. *IEEE Transactions on Geoscience and Remote Sensing*, 42(11), 2446–2453. https://doi.org/10.1109/tgrs.2004.835222

Karca, Ş. O., & Erten, G. (2023). Coseismic DInSAR Analysis and Elastic Dislocation Modelling of The 24 January 2020 Elazig-Sivrice Earthquake. *Turkish Journal of Remote Sensing*, 5(1), 1-13. https://doi.org/10.51489/tuzal.1187819

Lanari, R., Mora, O., Manunta, M., Mallorquí, J. J., Berardino, P., & Sansosti, E. (2004). A small-baseline approach for investigating deformations on full-resolution differential SAR interferograms. *IEEE Transactions on Geoscience and Remote Sensing*, 42(7), 1377-1386. https://doi.org/10.1109/TGRS.2004.828196

Liu, X., Cao, Q., Wang, S., & Anastasia, C. (2018). Optimized method for selecting common master image in PS-DInSAR. *Journal of Engineering Science and Technology Review*, 11(1), 208–215. https://doi.org/10.25103/jestr.111.25

Lu, Z., Kwoun, O., & Rykhus, R. (2007). Interferometric synthetic aperture radar (InSAR): Its past, present and future. *Photogrammetric Engineering & Remote Sensing*, 73(3), 217–221.

Martín-Antón, M., Negro, V., Del Campo, J. M., López-Gutiérrez, J. S., & Esteban, M. D. (2016). Review of coastal land reclamation situation in the world. *Journal of Coastal Research*, 75(sp1), 667–671. https://doi.org/10.2112/si75-133.1

Massonnet, D., & Feigl, K. L. (1998). Radar interferometry and its application to changes in the Earth's surface. *Reviews of Geophysics*, 36(4), 441–500. https://doi.org/10.1029/97rg03139

Pepe, A., Solaro, G., Calo, F., & Dema, C. (2016). A minimum acceleration approach for the retrieval of multiplatform InSAR deformation time series. *IEEE Journal of Selected Topics in Applied Earth Observations and Remote Sensing*, 9(8), 3883–3898. https://doi.org/10.1109/jstars.2016.2577878

Rucci, A., Ferretti, A., Guarnieri, A. M., & Rocca, F. (2012). Sentinel-1 SAR interferometry applications: The outlook for sub-millimeter measurements. *Remote Sensing of Environment*, 120, 156–163. https://doi.org/10.1016/j.rse.2011.09.030

Sefercik, U. G. (2013). Productivity of TerraSAR-X 3D data in urban areas: A case study in Trento. *European Journal of Remote Sensing*, 46(1), 597–612. https://doi.org/10.5721/eujrs20134635

Sefercik, U. G., Buyuksalih, G., & Atalay, C. (2020). DSM generation with bistatic TanDEM-X InSAR pairs and quality validation in inclined topographies and various land cover classes. *Arabian Journal of Geosciences*, 13, 560. https://doi.org/10.1007/s12517-020-05602-5

Shi, X., Zhong, J., Yin, Y., Chen, Y., Zhou, H., Wang, M., & Dai, K. (2023). Integrating SBAS-InSAR and LSTM for subsidence monitoring and prediction at Hong Kong international airport. *Ore and Energy Resource Geology*, 15, 100032. https://doi.org/10.1016/j.oreoa.2023.100032

Yu, C., Li, Z., & Penna, N. T. (2017a). Interferometric synthetic aperture radar atmospheric correction using a GPS-based iterative tropospheric decomposition model. *Remote Sensing of Environment*, 204, 109–121. https://doi.org/10.1016/j.rse.2017.10.038

Yu, C., Li, Z., Penna, N. T., & Crippa, P. (2018). Generic atmospheric correction model for interferometric synthetic aperture radar observations. *Journal of Geophysical Research: Solid Earth*, 123(10), 9202–9222. https://doi.org/10.1029/2017jb015305

Yu, C., Penna, N. T., & Li, Z. (2017b). Generation of real-time mode high-resolution water vapor fields from GPS observations. *Journal of Geophysical Research: Atmospheres*, 122(3), 2008–2025. https://doi.org/10.1002/2016jd025753

Zhao, C., Li, Z., Tian, B., Zhang, P., & Chen, Q. (2019). A ground surface deformation monitoring InSAR method using improved distributed scatterers phase estimation. *IEEE Journal of Selected Topics in Applied Earth Observations and Remote Sensing*, 12(11), 4543-4553. https://doi.org/10.1109/JSTARS.2019.2946729